Prepared for Medical Engineering & Physics

First submitted on August 28, 2012
Revision submitted on March 26, 2013
Final submitted on May 3, 2013

Influences of the Depth-dependent Material Inhomogeneity of Articular Cartilage on the Fluid Pressurization in the Human Knee

Y. Dabiri and L. P. Li *

Department of Mechanical and Manufacturing Engineering, University of Calgary,

2500 University Drive, N.W., Calgary, Alberta, Canada T2N 1N4

*Corresponding author:
LePing Li, Ph.D., P.Eng., Associate Professor
Department of Mechanical and Manufacturing Engineering
University of Calgary
2500 University Drive, N.W.
Calgary, Alberta, Canada T2N 1N4
Phone: 1 403 210 7537; Fax: 1 403 282 8406
Email: Leping.Li@ucalgary.ca

Abstract

The material properties of articular cartilage are depth-dependent, i.e. they differ in the superficial, middle and deep zones. The role of this depth-dependent material inhomogeneity in the poromechanical response of the knee joint has not been investigated with patient-specific joint modeling. In the present study, the depth-dependent and site-specific material properties were incorporated in an anatomically accurate knee model that consisted of the distal femur, femoral cartilage, menisci, tibial cartilage and proximal tibia. The collagen fibers, proteoglycan matrix and fluid in articular cartilage and menisci were considered as distinct constituents. The fluid pressurization in the knee was determined with finite element analysis. The results demonstrated the influences of the depth-dependent inhomogeneity on the fluid pressurization, compressive stress, first principal stress and strain along the tissue depth. The depth-dependent inhomogeneity enhanced the fluid support to loading in the superficial zone by raising the fluid pressure and lowering the compressive effective stress at the same time. The depth-dependence also reduced the tensile stress and strain at the cartilage-bone interface. The present 3D modeling revealed a complex fluid pressurization and 3D stresses that depended on the mechanical contact and relaxation time, which could not be predicted by existing 2D models from the literature. The greatest fluid pressure was observed in the medial condyle, regardless of the depth-dependent inhomogeneity. The results indicated the roles of the tissue inhomogeneity in reducing deep tissue fractures, protecting the superficial tissue from excessive compressive stress and improving the lubrication in the joint.

KEYWORDS: Articular cartilage mechanics; Cartilage heterogeneity; Collagen fiber orientation; Finite element analysis; Fluid pressure; Knee joint mechanics

Introduction

The major components of articular cartilage are collagen fibers, proteoglycans and synovial fluid [1, 2]. The compressive and shear stiffness of the tissue are governed by the proteoglycan matrix, while the tensile stiffness is governed by the collagen fibers. The collagen network also greatly contributes to the apparent compressive stiffness at fast loading through the fluid pressurization, which is enhanced by fiber reinforcement [3, 4]. The fluid is also responsible for the poromechanical behavior of the tissue [5]: the fluid pressure supports up to 90% of applied compressive loading [6], which reduces to an insignificant level at equilibrium. The cartilaginous tissues are commonly modeled as biphasic [7, 8].

The structure and properties of cartilage, e.g. fiber orientation and hydraulic permeability, change along the depth of the tissue from the articular surface to the bone interface [9, 10]. This change is referred to as depth-dependent material inhomogeneity, or zonal differences. The superficial zone is composed of fibers parallel to the articular surface, the fibers in the middle zone are not oriented in a specific direction, and the fibers in the deep zone are mainly perpendicular to the bone surface [10-12]. The importance of depth-dependent inhomogeneity has been the subject of experimental and theoretical studies [13-20]. These studies could be categorized into (1) simplified geometries that pertain to standard testing such as confined and unconfined compression tests [20], and (2) three-dimensional anatomically accurate geometries [21].

Concerning the first category, previous studies reported the importance of depth-dependence in the mechanical behavior of articular cartilage in unconfined compression tests [3, 22, 23]. The mechanical behavior of cartilage with depth-dependent properties in confined compression was also investigated simultaneously with unconfined compression [24, 25]. In addition, it was

reported that the alternation of permeability along the depth affected fluid pressurization and the mechanical behavior of the tissue [26].

The second category, three-dimensional models of human knee, has been developed to study the mechanical behavior of the knee in normal and pathological conditions [27-30]. Only two of the 3D models, however, have considered the material properties in a depth-dependent manner. The first one was an elastic model without fluid pressure [21]. The second one modeled the fluid pressure and zonal dependent fiber orientation to investigate the short-term load response [31], which is virtually elastic. The influence of the depth-dependence may not have been adequately shown in these two studies because of two reasons. First, the mechanical response of the tissue associated with the collagen network is more significant when substantial fluid pressure is present [3, 4, 32]. Second, the poromechanical response was not investigated. A previous study indicated more significant influence of fiber orientation during early relaxation [33].

Therefore, the objective of the present study was to determine what mechanical parameters of articular cartilage in the knee were affected by the depth-dependent material inhomogeneity. We were interested in fluid pressurization and dissipation in the tissues. An MRI-based knee joint model was used for this purpose. The collagen fibers, depth-dependent inhomogeneity, and fluid pressure were simultaneously considered for the cartilaginous tissues. In order to understand the significance of the depth-dependence, the results from the proposed model were compared with those obtained from a recently published model that did not include the depth-dependence [34]. The proposed model was otherwise the same as the published model: the fiber and fluid phases were particularly considered in both models.

Methods

A recently published knee joint model [34] was modified to include depth-dependent material properties in the femoral cartilage. The proposed model will be referred to as the inhomogeneous model, because both depth-dependent and site-specific material properties were incorporated. For the convenience of discussion, the published model will be referred to as the homogeneous model: it was homogeneous in the direction of the tissue thickness, although the site-specific material properties were also considered.

In the literature, the continuous variation of the depth-dependence is often characterized with three distinct zones. The superficial, middle and deep zones contain, respectively, 10%-20%, 40%-60% and almost 30% of the cartilage thickness [35, 36]. For the simplicity of the present inhomogeneous modeling, the three zones were taken to be approximately 25%, 50% and 25% of the cartilage thickness. They were further meshed with 2, 4 and 2 layers of elements respectively. Therefore, there were in total 8 layers of elements in the thickness direction. As the input of the finite element analysis, the fibers in the superficial zone were assumed to be in split-line directions [37]; the fibers in the middle zone were randomly distributed along the three directions, and the fibers in the deep zone were oriented perpendicular to the bone surface.

For the tibial cartilage, complete measurement data of fiber orientation were not found from the literature, although split-lines in the submeniscal region were arranged in a wheel-spoke pattern [38]. Therefore, the mechanical properties were assumed the same for all directions, i.e. no preferred fiber orientation was considered for the tibial cartilage. For the meniscus, the fibers were incorporated primarily in the circumferential and secondly in the radial directions [39].

The constitutive behavior of the tissues is described by a fibril-reinforced model previously published [23]. Some equations are included here for the convenience of reading. The total stress

in the tissue, which is the stress in the mixture, is determined by the fluid pressure, p, and the effective stress of the solid matrix, $\boldsymbol{\sigma}^{eff}$

$$\boldsymbol{\sigma} = -p\mathbf{I} + \boldsymbol{\sigma}^{eff} \tag{1}$$

where the effective stress consists of the effective stress of the orthotropic fibrillar matrix, $\boldsymbol{\sigma}^{f}$, and the effective stress of the isotropic nonfibrillar matrix defined by the Lamé constants λ and μ

$$\boldsymbol{\sigma}^{eff} = \lambda e\mathbf{I} + 2\mu\boldsymbol{\varepsilon} + \boldsymbol{\sigma}^{f} \tag{2}$$

where e is the volumetric strain and $\boldsymbol{\varepsilon}$ is the strain. The fibrillar matrix mimics the collagen network, while the nonfibrillar matrix mimics the proteoglycan matrix. As a first approximation, the fibrillar stress is neglected if the tissue is in compression in the fibre direction. The tensile stress in the fibrillar matrix is determined by [33]

$$\mathrm{d}\sigma_x^f = E_x^f \, d\varepsilon_x \tag{3}$$

where E_x^f is the fibrillar modulus in the x-direction, which aligns in the direction of fibres or primary fibres. For the case of small fibrillar strains,

$$E_x^f = E_x^0 + E_x^{\varepsilon} \, \varepsilon_x \tag{4}$$

where E_x^0 and E_x^{ε} are direction- and depth-dependent constants. Replacing x with y and z, respectively, will derive the corresponding equations for the transverse directions. Obviously, this formula will not be valid when the tensile strain is large. Fortunately, when cartilage is compressed from the articular surface, the lateral tensile strain is only a fraction of the compressive strain. Therefore, this simple formula can approximate moderate compressions.

The Lamé constants λ and μ in equation (2) can be replaced by the Young's modulus and Poisson's ratio, E_m and ν_m, of the nonfibrillar matrix. For the inhomogeneous model, the two parameters for the femoral cartilage were approximated as linear functions of the tissue depth z

$$E_m = \hat{E}_m\left(1+\alpha_E \, z/h\right), \quad \nu_m = \hat{\nu}_m\left(1+\alpha_\nu \, z/h\right) \tag{5}$$

where $\hat{E}_m$ and $\hat{\nu}_m$ are respectively the Young's modulus and Poisson's ratio at the articular surface; *h* is the tissue thickness; α_E and α_ν are positive constants. This equation was proposed in a previous study [23] based on data from the literature [20, 40].

Darcy's law was used to describe the fluid flow in the tissues. The permeability of the femoral cartilage was assumed to increase from the superficial zone to middle zone, and then decrease through the deep zone [9, 26, 41]. The material properties for the tibial cartilage, menisci and bones were the same as what were used in a previous study [34]. The material properties for all tissues are summarized in Table 1. When these properties were combined with the site-specific fiber orientation, the spatial inhomogeneity was incorporated, i.e. both depth-dependence and site-dependence were considered in the inhomogeneous model.

The surface-to-surface contact (ABAQUS manual) was defined between the following contact pairs: femoral cartilage (master surface) and meniscus, femoral (master surface) and tibial cartilages, and tibial cartilage (master surface) and meniscus. Using the TIE option in ABAQUS, the following tissues were attached to each other at their interfaces: femoral cartilage to femoral distal surface, and tibial cartilage to tibial proximal surface. The ends of menisci were fixed to the tibial proximal surface using the TIE option, too.

Pore pressure elements were used to mesh cartilages and menisci, and solid elements were used to mesh bones. The 20-node hexahedral elements (C3D20P) were used for the femoral cartilage, and 8-node hexahedral elements (C3D8P) were used for meniscus and tibia cartilage. This choice had the potential of better fluid pressure results for the femoral cartilage, and yet good numerical convergence in the contact modeling, since the 20-node elements experienced more difficulties in the contact convergence than the 8-node elements (as stated in the ABAQUS manual). The femur and tibia were meshed using 4-node tetrahedral elements to better approximate the surface geometries of the bones than using the hexahedral elements.

The *soil consolidation* procedure in ABAQUS was used to simulate the stress relaxation in the tissues. The procedure was initially developed for the calculation of soil settlement, but has been widely used to account for the transient response of biological tissues. A ramp compression of the knee of 0.5 mm was applied at 0.1 mm/s, and then held unchanged for 400 seconds (stress relaxation). The bottom of tibia was fixed while the displacement was applied on the top of the femur. The femur was not constrained in rotations, but its top was constrained against translations in the transverse plane. The part of distal femur in consideration was 104 mm in height [34]. Therefore, the constraints on the top still allowed considerable sliding between the articulating surfaces. The fluid pressure was given to be zero at the articular surface, if it was not in contact with its mating surface.

To assess the role of depth-dependent inhomogeneity on the contact mechanics of the joint, the homogeneous model was also considered with constant properties along the direction of the tissue thickness. In the homogeneous model, the fiber orientation in all zones was assumed to be the same as the split-line direction [37], noting that the split-lines were site-specific. The material properties for the homogeneous model (Table 2) were chosen so that the reaction forces at maximum compression were virtually identical for the homogeneous and inhomogeneous models (Fig. 1).

Results

The results are mainly presented for the femoral cartilage, because the depth-dependent properties were implemented in this tissue. The total forces obtained from the two models are very close after careful selection of the material properties for the homogeneous model (Fig. 1). In our preliminary study, we attempted to match the force at 0.1mm compression using a

different elastic modulus for the homogeneous model. The two force curves deviated from each other soon after the ramp compression, resulting in 10% difference at equilibrium (not shown).

The depth variations of short-term and long-term fluid pressures are shown for a central contact location (Figs. 2a,b). For better understanding of the mechanism of fluid pressurization, the compressive effective stress is also presented (Figs. 2c,d). The total compressive stress in the tissue thickness direction is the sum of this stress and the fluid pressure (Equation (1)). In either model prediction, the depth variation of the compressive stress was opposite to that of fluid pressure (Figs. 2c vs 2a; 2d vs 2b). For instance, the compressive stress *increased with the depth* (Fig. 2d), while the fluid pressure *decreased with the depth* (Fig. 2b).

The first principal stress and strain are tensile and mainly produced by the lateral expansion when it is compressed in the perpendicular direction (Figs. 3). However, at the cartilage-bone interface, they were greatly influenced by the shearing at the interface. So their variations were different there (Fig. 3). The first principal stress here was calculated from the effective stresses. This stress must be subtracted by the fluid pressure in order to obtain the total principal stress in the tissue as a mixture, because the effective stress is now positive but the pressure is negative by nature (Equation (1)).

The fluid pressure contours are shown for a sagittal section and a coronal section of the contact region (Figs. 4 & 5). For the case of the inhomogeneous model, the maximum pressure in each of the contours is shown with the maximum value in the corresponding legend. For the case of the homogeneous model, the exact value of the maximum pressure is not actually shown in the figure. They are, therefore, included in the figure captions.

For both model predictions, the fluid pressures in the central contact region were generally greater in the superficial zone than that in the deep zone (Figs. 6b vs 6a; Fig. 4). However, the pressures also decayed faster in the superficial zone so that the long-term pressures were more

uniform along the depth than short-term pressures (Figs. 6, 4 and 5). The maximum fluid pressure occurred in the medial condyle, regardless the layers and material models that were considered (Figs. 7 & 8).

Discussion

The depth-dependent material inhomogeneity enhanced the fluid pressure and pressure gradient in the superficial zone of the contact region with less significant influence on the pressurization in the middle and deep zones. This is observed when the fluid pressures predicted by the inhomogeneous and homogeneous models are compared (Figs. 2a,b, 4 & 5). With the inhomogeneous material properties, fiber orientations in the tissue are favorable to the fluid pressurization in the superficial zone. Our results are consistent with what has been reported for tissue discs under uniform compression [3] and for a hexahedral tissue block under indentation [33]. Our results also support qualitatively the conclusion from an independent study [42] that inhomogeneous cartilage properties enhance superficial interstitial fluid support. However, both our homogeneous and inhomogeneous models predicted slightly higher pressures in the superficial layer of the central contact region as compared to that in the deep layer. In the reported study [42], the homogeneous model predicted a lower fluid pressure in the superficial layer as compared to that in the deep zone, while the inhomogeneous model predicted similar fluid pressures in the superficial and deep layers. This difference in the depth-varying fluid pressures could have been produced by the different contact geometries and constitutive models considered in the two studies. In the reported study [42], the indentation of a flat piece of tissue with a spherical indentor was simulated using the conewise linear elastic constitutive model. In the present study, a more realistic knee joint contact was simulated including the menisci. The use of a fibril-reinforced constitutive model in the present study should also have highlighted the

role of the collagen network in the fluid pressurization in the tissue. It must be noted that the depth variation of the fluid pressure is different in other regions. For example, the surface pressure is close to zero at the border of the contact region, but higher in the deep layers there (Figs 4 and 5).

Articular cartilage in situ exhibited more complex behavior than the explants in vitro. The present 3D modeling revealed a complex fluid pressurization and 3D stresses that depended on the mechanical contact and relaxation time, which could not be predicted by existing 2D models from the literature. The depth-varying fluid pressure in the outer contact region and noncontact region were different from that in the central contact region (Figs. 4 and 5). The pressure distribution in the sagittal plane was different from that in the coronal plane (Figs. 4 and 5). Furthermore, the depth-varying fluid pressure altered with stress relaxation (the results for 5s vs 400s in Fig. 4 or 5). Both the magnitude and distribution of the fluid pressure were less sensitive to the depth-dependent inhomogeneity at longer times (Figs. 2b, 2d, 4b & 5b, 400s). The tensile strain was the highest in the superficial zone (Fig. 3c,d), which cannot be modeled using a cartilage disk [23] because of the differences in boundary conditions. Optical measurement with tissue disks showed maximum tensile strain in the deep layer, and smallest in the superficial layer [48].

The stresses in the tissue matrix were modulated by the fluid pressurization [49,50]. A raised fluid pressure in the superficial zone reduced the effective stress in the tissue matrix - the depth variation of the compressive stress was opposite to that of fluid pressure (Fig. 2). This fluid pressure mechanism is believed to protect the tissue matrix from excessive stresses. The material inhomogeneity enhanced this mechanism. When it is not pressurized, the superficial tissue is softer than the deeper tissue, which is favorable for joint motion. The raised fluid pressure in the superficial zone enhanced the load support of the softer tissue in the superficial zone. In general,

the ratio of the fluid pressure to solid stress in the superficial zone was higher in the inhomogeneous model than the homogeneous one (Figs. 2a vs 2c; 2b vs 2d), which implied reduced frictions by the depth-dependent material inhomogeneity [43-46].

The depth-dependent material inhomogeneity caused a stress concentration between the superficial and middle zones (Fig. 3a,b). This must be partially produced by the implementation of discontinuous material properties there, especially the change in the collagen fiber orientation. In reality, however, there is no distinct boundary between the two zones. Therefore, the stress there must have been overestimated. A more accurate prediction requires the implementation of material properties that continuously vary over the tissue thickness. The first principal strain, however, monotonically reduced with the tissue depth until the cartilage-bone interface (Fig. 3c,d). The maximum tensile strain in the deep zone was less than half of that in the superficial zone. These results might indicate that the zonal differences protected the deep layers and cartilage-bone interface from excessive stress and strain (Fig. 3), which was in line with the in vitro result that superficial layers played a protective role for deep layers [26]. The deep layer fractures occurred frequently [47]. Normal depth-dependent properties may reduce the occurrence of the fractures.

The fluid pressure distribution within a cartilage layer parallel to the articular surface was similar in pattern for the homogenous and inhomogeneous models (Figs. 8 vs 7), but somewhat dependent on the relaxation time (not shown). The distribution was determined by the site-specific fiber orientation which were the same in the two material models. These results indicate the possibility of using the *homogeneous* model (which is homogenous in the depth direction but site-specific) to predict certain mechanical responses of the knee, as long as these differences are taken into consideration when the results are interpreted. When a homogeneous model was used, 4 layers of elements yielded fast converged results [34].

A few limitations exist in the current modeling. First, only 8 layers of elements were used in the present study, which was not accurate enough for describing the large depth variations in stresses and pressures (Figs. 2 & 3). This limitation might have produced some numerical errors in variables with large gradients in the tissue thickness direction, such as stress concentrations (Fig. 3a,b). When more layers of elements were used, however, we experienced extremely slow numerical convergence with the very thin elements. It was not simply the issue with the increased degrees of freedom, but more trouble with the tolerance of contact convergence. The use of 8 layers of elements gave us some quality results, although smoother depth variations would be obtained, if more layers were meshed in the tissue thickness direction. Furthermore, accurate representation of the depth variations requires the segmentation of the three zones with intensive imaging analysis, although such techniques are available [51].

Another limitation of the study was the use of non-physiological loading, which made it possible to obtain some simple results. Furthermore, we have simulated stress relaxation other than creep loading in order to speed up the computation, because a creep testing would take much more time to complete [52,53]. For the sake of fast convergence as well, the ramp compression was applied in 5s rather than in a shorter, realistic time (0.5-1s). Therefore, the fluid pressure and the tensile stresses have been underestimated. Even with these simplifications, it took approximately one month to complete a single computation. Our current goal is to understand the fundamental mechanism of the poromechanical response of the knee joint. We wish to determine the mechanics under simple loadings and gain experiences in this type of modeling before moving to more realistic problems. These simplifications do not seem to compromise this goal.

The use of a small deformation theory is another key factor leading to reduced convergence complexities. In a previous study [54], the sensitivity of three nonlinear factors to the load response was investigated, i.e. nonlinear fibrillar property, nonlinear permeability and large

deformation. It was found that the combined effect of nonlinear permeability and large deformation on the results was not nearly as significant as that of the nonlinear fibrillar property. The model was able to describe experimental data only when the nonlinear fibrillar property was considered. Therefore, the effect of large deformation was ignored but the fibrillar nonlinearity was considered in the present study. However, this simplification will only affect the magnitudes of the results, e.g. the predicted fluid pressure could be somewhat underestimated. The qualitative results and conclusion would remain the same, should a large deformation theory be used.

The constitutive model used in the present study has been previously validated against multiple experimental data in unconfined compression and tensile testing, such as simultaneous prediction of creep and relaxation in unconfined compression [52]. The tissue model was able to account for the great ratios of the transient versus equilibrium load responses observed in experiments [52,54]. The strong transient response is believed to be caused by the interplay between fibril reinforcement and fluid pressurization [54,55]. Therefore, collagen fibers and fluid pressure were incorporated in the present knee model. Collagen fibril reinforcement, however, must be interpreted as a mathematical approximation of the complex structure of the tissues.

Published studies on the mechanical behavior of articular cartilage associated with the zonal differences were limited to either simple explants geometries with the inclusion of fluid pressure [22, 25, 42], or realistic knee contact geometry with elastic or nearly elastic response [21, 31]. We have implemented the depth-dependent material inhomogeneity in an anatomically accurate knee contact model including the fluid flow and pressure, as well as the site-specific fiber orientation. The poromechanical response of the knee joint was also investigated. Some of the present results were qualitatively similar to those obtained from the explants, e.g. the depth-dependent material inhomogeneity enhanced the fluid pressurization in the superficial zone [42]. Other results, such as the 3D fluid pressures and 3D stress concentrations, as well as the spatial

distribution of tensile strain reduction at the cartilage-bone interface, could only be obtained using the current 3D modeling. These findings may be applied in the studies of osteoarthritis and cartilage tissue engineering [6], after the modeling has been extended with more realistic loadings.

ACKNOWLEDGEMENTS

Competing interests: None declared

Funding: Natural Sciences and Engineering Research Council of Canada, and the Canadian Institutes of Health Research

Ethical approval: E-22593, University of Calgary, for the use of MRI of human subjects

REFERENCES

[1] Mow V, Ratcliffe A, Structure and function of articular cartilage and meniscus, in *Basic orthopaedic biomechanics*, Mow V and Hayes W, Eds., Second ed: Lippincott-Hayes, 1997, pp. 113-177.

[2] Mow VC, Kuei SC, Lai WM, Armstrong CG, Biphasic creep and stress relaxation of articular cartilage in compression? Theory and experiments. J Biomech Eng 1980; 102: 73-84.

[3] Li LP, Shirazi-Adl A, Buschmann MD, Alterations in mechanical behaviour of articular cartilage due to changes in depth varying material properties--a nonhomogeneous poroelastic model study. Comput Methods Biomech Biomed Engin 2002; 5: 45-52.

[4] Mizrahi J, Maroudas A, Lanir Y, Ziv I, Webber TJ, The "instantaneous" deformation of cartilage: effects of collagen fiber orientation and osmotic stress. Biorheology 1986; 23: 311-30.

[5] Mow VC, Fithian DC, Kelly MA, Fundamentals of articular cartilage and meniscus biomechanics, in *Articular Cartilage and Knee Joint Function: Basic Science and Arthroscopy*, Ewing JW, Ed., ed New York: Raven Press, 1990, pp. 1-18.

[6] Ateshian GA, Hung CT, Patellofemoral joint biomechanics and tissue engineering. Clin Orthop Relat Res 2005; 81: 81-90.

[7] Mow VC, Mansour JM, The nonlinear interaction between cartilage deformation and interstitial fluid flow. J Biomech 1977; 10: 31-9.

[8] Mak AF, Lai WM, Mow VC, Biphasic indentation of articular cartilage--I. Theoretical analysis. J Biomech 1987; 20: 703-14.

[9] Maroudas A, Bullough P, Permeability of articular cartilage. Nature 1968; 219: 1260-1.

[10] Minns RJ, Steven FS, The collagen fibril organization in human articular cartilage. J Anat 1977; 123: 437-57.

[11] Jeffery AK, Blunn GW, Archer CW, Bentley G, Three-dimensional collagen architecture in bovine articular cartilage. J Bone Joint Surg Br 1991; 73: 795-801.

[12] Weiss C, Rosenberg L, Helfet AJ, An ultrastructural study of normal young adult human articular cartilage. J Bone Joint Surg Am 1968; 50: 663-74.

[13] Chegini S, Ferguson SJ, Time and depth dependent Poisson's ratio of cartilage explained by an inhomogeneous orthotropic fiber embedded biphasic model. J Biomech 2010; 43: 1660-6.

[14] Chen AC, Bae WC, Schinagl RM, Sah RL, Depth- and strain-dependent mechanical and electromechanical properties of full-thickness bovine articular cartilage in confined compression. J Biomech 2001; 34: 1-12.

[15] Chen SS, Falcovitz YH, Schneiderman R, Maroudas A, Sah RL, Depth-dependent compressive properties of normal aged human femoral head articular cartilage: relationship to fixed charge density. Osteoarthritis Cartilage 2001; 9: 561-9.

[16] Federico S, Herzog W, On the anisotropy and inhomogeneity of permeability in articular cartilage. Biomech Model Mechanobiol 2008; 7: 367-78.

[17] Mow VC, Guo XE, Mechano-electrochemical properties of articular cartilage: their inhomogeneities and anisotropies. Annu Rev Biomed Eng 2002; 4: 175-209.

[18] Julkunen P, Kiviranta P, Wilson W, Jurvelin JS, Korhonen RK, Characterization of articular cartilage by combining microscopic analysis with a fibril-reinforced finite-element model. J Biomech 2007; 40: 1862-70.

[19] Saarakkala S, Julkunen P, Kiviranta P, Mäkitalo J, Jurvelin JS, Korhonen RK, Depth-wise progression of osteoarthritis in human articular cartilage: investigation of composition, structure and biomechanics. Osteoarthritis Cartilage 2010; 18: 73-81.

[20] Schinagl RM, Gurskis D, Chen AC, Sah RL, Depth-dependent confined compression modulus of full-thickness bovine articular cartilage. J Orthop Res 1997; 15: 499-506.

[21] Shirazi R, Shirazi-Adl A, Hurtig M, Role of cartilage collagen fibrils networks in knee joint biomechanics under compression. J Biomech 2008; 41: 3340-8.

[22] Korhonen RK, Julkunen P, Wilson W, Herzog W, Importance of collagen orientation and depth-dependent fixed charge densities of cartilage on mechanical behavior of chondrocytes. J Biomech Eng 2008; 130: 021003.
[23] Li LP, Buschmann MD, Shirazi-Adl A, A fibril reinforced nonhomogeneous poroelastic model for articular cartilage: inhomogeneous response in unconfined compression. J Biomech 2000; 33: 1533-41.
[24] Wilson W, van Donkelaar CC, van Rietbergen B, Ito K, Huiskes R, Stresses in the local collagen network of articular cartilage: a poroviscoelastic fibril-reinforced finite element study. J Biomech 2004; 37: 357-66.
[25] Wilson W, van Donkelaar CC, van Rietbergen R, Huiskes R, The role of computational models in the search for the mechanical behavior and damage mechanisms of articular cartilage. Med Eng Phys 2005; 27: 810-26.
[26] Setton LA, Zhu W, Mow VC, The biphasic poroviscoelastic behavior of articular cartilage: role of the surface zone in governing the compressive behavior. J Biomech 1993; 26: 581-92.
[27] Bendjaballah MZ, Shirazi-AdI A, Zukor DJ, Biomechanics of the human knee joint in compression: reconstruction, mesh generation and finite element analysis. Knee 1995; 2: 69-79.
[28] Peña E, Calvo B, Martínez MA, Palanca D, Doblaré M, Finite element analysis of the effect of meniscal tears and meniscectomies on human knee biomechanics. Clin Biomech (Bristol, Avon) 2005; 20: 498-507.
[29] Peña E, Calvo B, Martínez MA, Doblaré M, Computer simulation of damage on distal femoral articular cartilage after meniscectomies. Comput Biol Med 2008; 38: 69-81.
[30] Périé D, Hobatho MC, In vivo determination of contact areas and pressure of the femorotibial joint using non-linear finite element analysis. Clin Biomech (Bristol, Avon) 1998; 13: 394-402.
[31] Mononen ME, Mikkola MT, Julkunen P, Ojala R, Nieminen MT, Jurvelin JS, *et al.*, Effect of superficial collagen patterns and fibrillation of femoral articular cartilage on knee joint mechanics-a 3D finite element analysis. J Biomech 2012; 45: 579-87.
[32] Oloyede A, Flachsmann R, Broom ND, The dramatic influence of loading velocity on the compressive response of articular cartilage. Connect Tissue Res 1992; 27: 211-24.
[33] Li LP, Cheung JT, Herzog W, Three-dimensional fibril-reinforced finite element model of articular cartilage. Med Biol Eng Comput 2009; 47: 607-15.
[34] Gu KB, Li LP, A human knee joint model considering fluid pressure and fiber orientation in cartilages and menisci. Med Eng Phys 2011; 33: 497-503.
[35] Mow VC, Ratcliffe A, Poole AR, Cartilage and diarthrodial joints as paradigms for hierarchical materials and structures. Biomaterials 1992; 13: 67-97.
[36] Newman AP, Articular cartilage repair. Am J Sports Med 1998; 26: 309-24.
[37] Below S, Arnoczky SP, Dodds J, Kooima C, Walter N, The split-line pattern of the distal femur: A consideration in the orientation of autologous cartilage grafts. Arthroscopy 2002; 18: 613-7.
[38] Goodwin DW, Wadghiri YZ, Zhu H, Vinton CJ, Smith ED, Dunn JF, Macroscopic structure of articular cartilage of the tibial plateau: influence of a characteristic matrix architecture on MRI appearance. AJR Am J Roentgenol 2004; 182: 311-8.
[39] Fithian DC, Kelly MA, Mow VC, Material properties and structure-function relationships in the menisci. Clin Orthop Relat Res 1990; 252: 19-31.
[40] Schinagl RM, Ting MK, Price JH, Sah RL, Video microscopy to quantitate the inhomogeneous equilibrium strain within articular cartilage during confined compression. Ann Biomed Eng 1996; 24: 500-12.
[41] Muir H, Bullough P, Maroudas A, The distribution of collagen in human articular cartilage with some of its physiological implications. J Bone Joint Surg Br, 1970; 52: 554-63.
[42] Krishnan R, Park S, Eckstein F, Ateshian GA, Inhomogeneous cartilage properties enhance superficial interstitial fluid support and frictional properties, but do not provide a homogeneous state of stress. J Biomech Eng 2003; 125: 569-77.
[43] Ateshian GA, The role of interstitial fluid pressurization in articular cartilage lubrication. J Biomech 2009; 42: 1163-76.

[44] Ateshian G, Wang H, Lai W, The role of interstitial fluid pressurization and surface porosities on the boundary friction of articular cartilage. Journal of Tribology-Transactions of the ASME 1998; 120: 241-248.
[45] Forster H, Fisher J, The influence of loading time and lubricant on the friction of articular cartilage. Proc Inst Mech Eng 1996; 210: 109-119.
[46] McCutchen CW, The frictional properties of animal joints. Wear 1962; 5: 1-17.
[47] Meachim G, Bentley G, Horizontal splitting in patellar articular cartilage. Arthritis Rheum 1978; 21: 669-74.
[48] Jurvelin JS, Buschmann MD, Hunziker EB, Optical and mechanical determination of Poisson's ratio of adult bovine humeral articular cartilage. J Biomech 1997; 30: 235-41.
[49] Oloyede A, Broom N, Is classical consolidation theory applicable to articular cartilage deformation? Clinical Biomechanics 1991; 6: 206-212.
[50] Oloyede A, Broom N, Stress-sharing between the fluid and solid components of articular cartilage under varying rates of compression. Connect Tissue Res 1993; 30: 127-41.
[51] Potter HG, Black BR, Chong LR, New techniques in articular cartilage imaging. Clin Sports Med 2009; 28: 77–94. doi:10.1016/j.csm.2008.08.004.
[52] Li LP, Korhonen RK, Iivarinen J, Jurvelin JS, Herzog W, Fluid pressure driven fibril reinforcement in creep and relaxation tests of articular cartilage. Med Eng Phys 2008; 30: 182-89.
[53] Kazemi M, Dabiri Y, Li LP, Recent advances in computational mechanics of the human knee joint. Computational and Mathematical Methods in Medicine; 2013: 27 pages, doi: 10.1155/2013/718423.
[54] Li LP, Soulhat J, Buschmann MD, Shirazi-Adl A, Nonlinear analysis of cartilage in unconfined ramp compression using a fibril reinforced poroelastic model. Clin Biomech (Bristol, Avon) 1999; 14: 673-82.
[55] Li LP, Shirazi-Adl A, Buschmann MD, Investigation of mechanical behavior of articular cartilage by fibril reinforced poroelastic models. Biorheology 2003; 40: 227-33.

Table 1. Material properties for all tissues used in the *inhomogeneous* model (Modulus: MPa; Permeability: 10^{-3}mm^4/Ns). The *x* is the primary fiber direction, i.e. the split-line direction for the superficial zone, the depth direction for the deep zone, and the circumferential direction for the meniscus. The *y* and *z* are perpendicular to the primary fiber direction in the local coordinate system. The material properties in the *y* and *z* directions are assumed to be the same. Thus a symbol, *y*/*z*, is used to denote either *y* or *z* direction.

Tissue		Fibrillar matrix		Nonfibrillar matrix		Permeability	
		E_x	$E_{y/z}$	E_m	ν_m	x	y / z
Femoral cartilage	Deep	$3+1600\varepsilon_x$	$0.9+480\varepsilon_{y/z}$	0.80	0.36	1.0	0.5
	Middle	$2+1000\varepsilon_x$	$2+1000\varepsilon_{y/z}$	0.60	0.30	3.0	1.0
	Superficial	$4+2200\varepsilon_x$	$1.2+660\varepsilon_{y/z}$	0.20	0.16	1.0	0.5
Tibial cartilage		$2+1000\varepsilon_x$	$2+1000\varepsilon_{y/z}$	0.26	0.36	2.0	1.0
Menisci		28	5	0.50	0.36	2.0	1.0
Bones		E = 5000		ν = 0.30			

Table 2. Material properties for the femoral cartilage in the *homogeneous* model (Modulus: MPa; Permeability: 10^{-3}mm^4/Ns). The x is the primary fiber direction. The properties for the tibial cartilage, menisci and bones are the same as shown in Table 1 for the *inhomogeneous* model.

Tissue	Fibrillar matrix		Nonfibrillar matrix		Permeability	
	E_x	$E_{y/z}$	E_{m}	ν_{m}	x	y / z
Femoral cartilage	$3+1600\varepsilon_x$	$0.9+480\varepsilon_{y/z}$	0.55	0.36	2.0	1.0

Figure Captions

Fig 1. Total reaction force in the knee joint as a function of time. A ramp compression of 500μm was applied in 5s followed by relaxation. The material properties for the *homogeneous* model were chosen so that the corresponding force obtained was the same as that predicted by the *inhomogeneous* model at 500μm compression, as marked by the star.

Fig 2. Variation of fluid pressure and compressive stress (MPa) along the depth of the femoral cartilage, shown for a location in the central contact region of the lateral condyle. The compressive stress refers to the normal stress of the matrix in the direction of cartilage thickness (positive = compressive). Results were calculated at the centroids of the elements (middle of each layer of elements). The depth is normalized by the thickness (0 = articular surface; 1 = bone interface).

Fig 3. First principal stress or strain along the depth of the femoral cartilage, shown for a location in the central contact region of the lateral condyle (positive = tensile). Results were calculated at the centroids of the elements (middle of each layer of elements). The depth is normalized by the thickness (0 = articular surface; 1 = bone interface).

Fig. 4. Fluid pressure in the sagittal plane of the femoral cartilage that is cut through the medial condyle. (a) at 20 s, and (b) at 400 s. The articular surface is shown at the bottom side; the posterior side is on the left. For the homogeneous case, the maximum pressures at 20 and 400s were 1.617 and 0.459 MPa respectively.

Fig. 5. Fluid pressure in the coronal plane of the femoral cartilage that is cut through the medial condyle only. (a) at 20 s, and (b) at 400 s. The articular surface is shown at the bottom side; the

lateral side is on the left. For the homogeneous case, the maximum pressures at 20 and 400 s were 1.617 and 0.590 MPa respectively.

Fig. 6. Maximum fluid pressure in a given layer of elements. (a) at the normalized depth of 13/16 (center of the 7^{th} layer, deep zone), and (b) at the normalized depth of 3/16 (center of 2^{nd} layer, superficial zone). The peak value shown in (a) are 1.676 and 1.657 MPa, respectively, for the *inhomogeneous* and *homogeneous* cases; the peak values shown in (b) are 1.880 and 1.758 MPa, respectively, for the *inhomogeneous* and *homogeneous* cases.

Fig. 7. Fluid pressure at 100 s as predicted by the *inhomogeneous* model at the normalized depth of (a) 13/16, and (b) 3/16 (0 = articular surface).

Fig. 8. Fluid pressure at 100 s as predicted by the *homogeneous* model at the normalized depth of (a) 13/16, and (b) 3/16 (0 = articular surface).

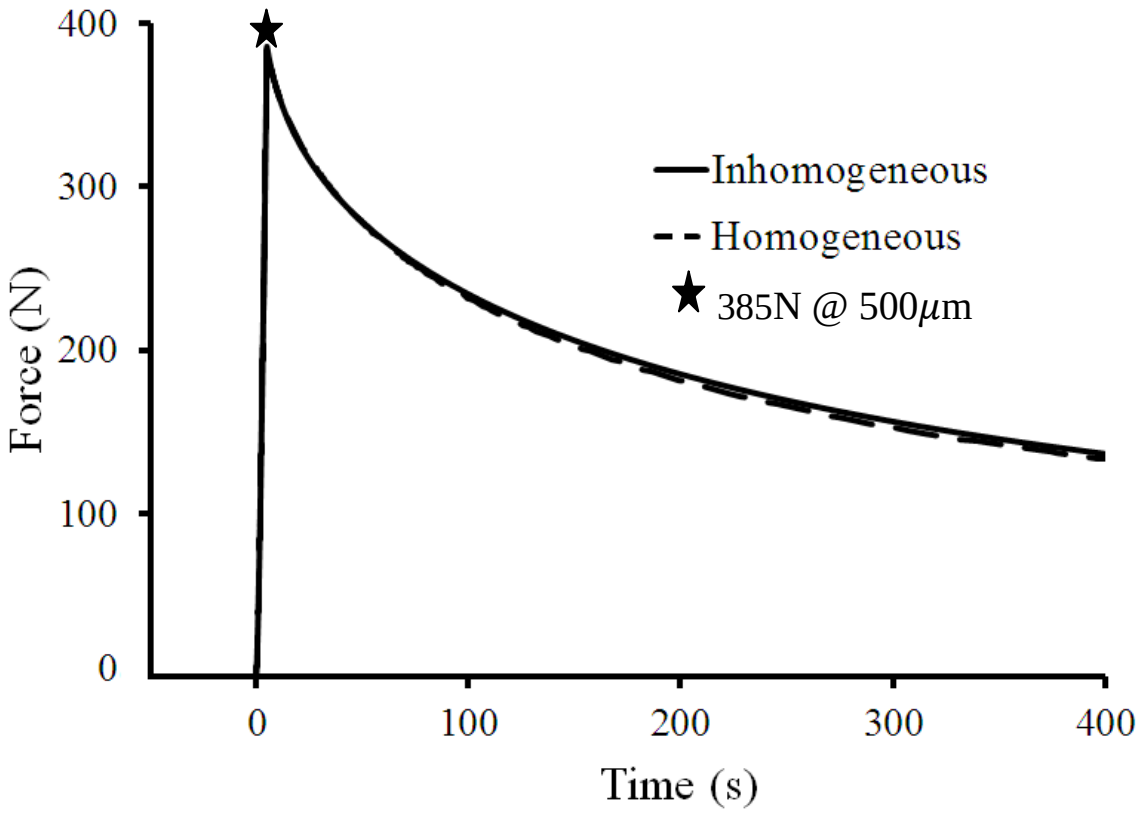
400
300
200
100
0
Force (N)
0
100
200
300
400
Time (s)
Inhomogeneous
Homogeneous
385N @ 500μm

Fig. 1

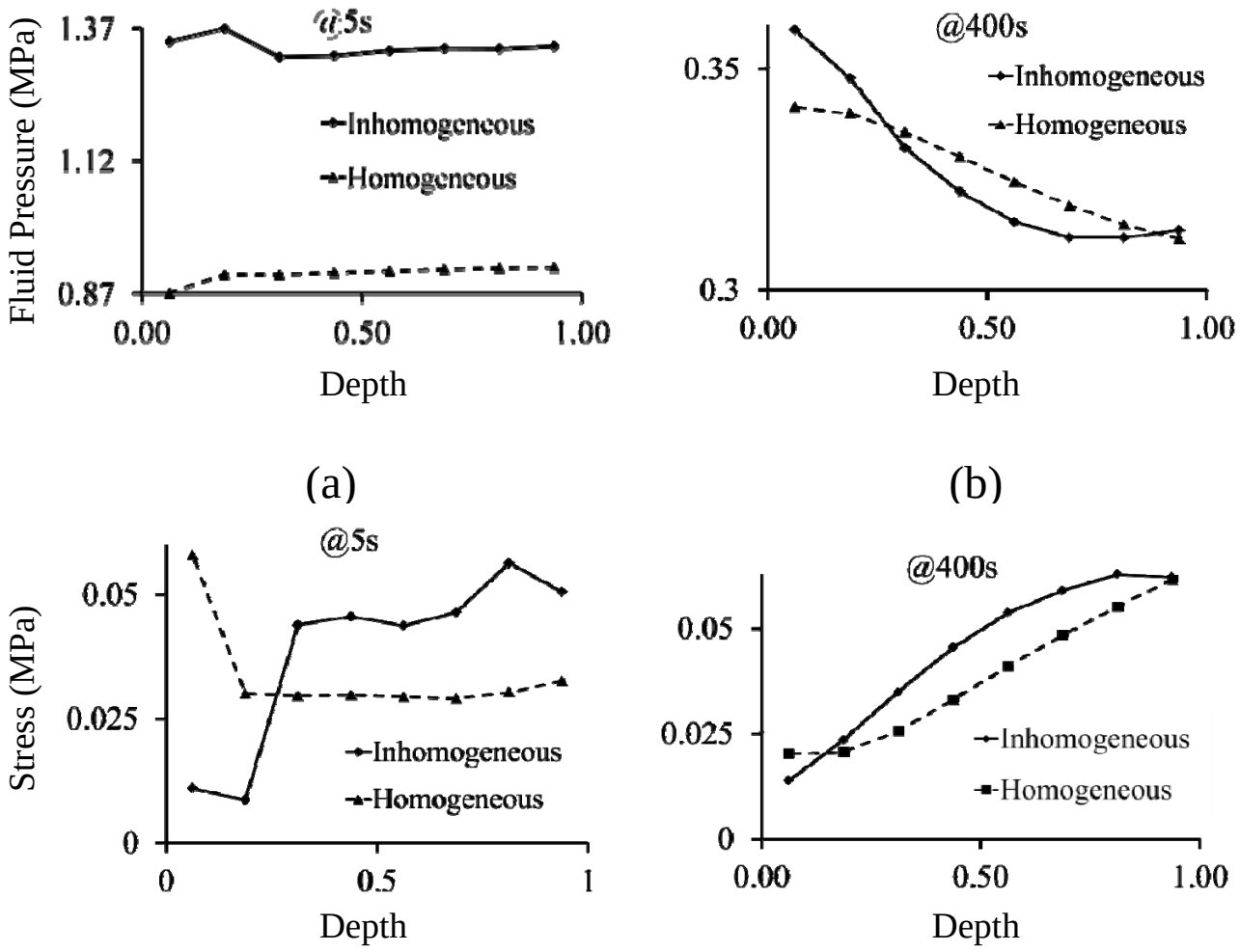
Fluid Pressure (MPa)
1.37
1.12
0.87
@5s
Inhomogeneous
Homogeneous
0.00
0.50
1.00
Depth
(a)
0.35
0.3
@400s
Inhomogeneous
Homogeneous
0.00
0.50
1.00
Depth
(b)
Stress (MPa)
0.05
0.025
0
@5s
Inhomogeneous
Homogeneous
0
0.5
1
Depth
(c)
0.05
0.025
0
@400s
Inhomogeneous
Homogeneous
0.00
0.50
1.00
Depth
(d)

Fig. 2

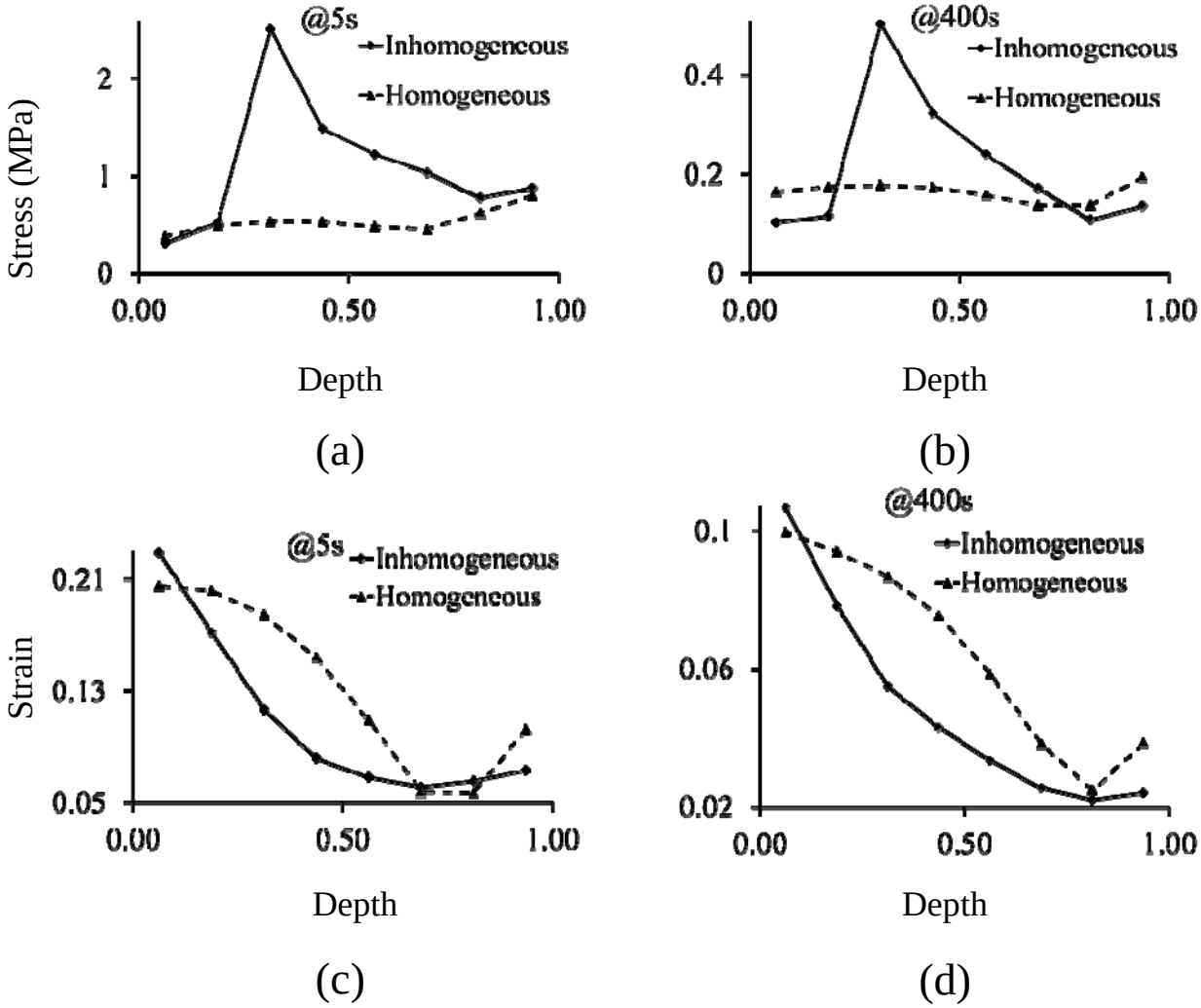
@5s
Inhomogeneous
Homogeneous
Stress (MPa)
2
1
0
0.00
0.50
1.00
Depth
(a)
@400s
Inhomogeneous
Homogeneous
0.4
0.2
0
0.00
0.50
1.00
Depth
(b)
@5s
Inhomogeneous
Homogeneous
Strain
0.21
0.13
0.05
0.00
0.50
1.00
Depth
(c)
@400s
Inhomogeneous
Homogeneous
0.1
0.06
0.02
0.00
0.50
1.00
Depth
(d)

Fig. 3

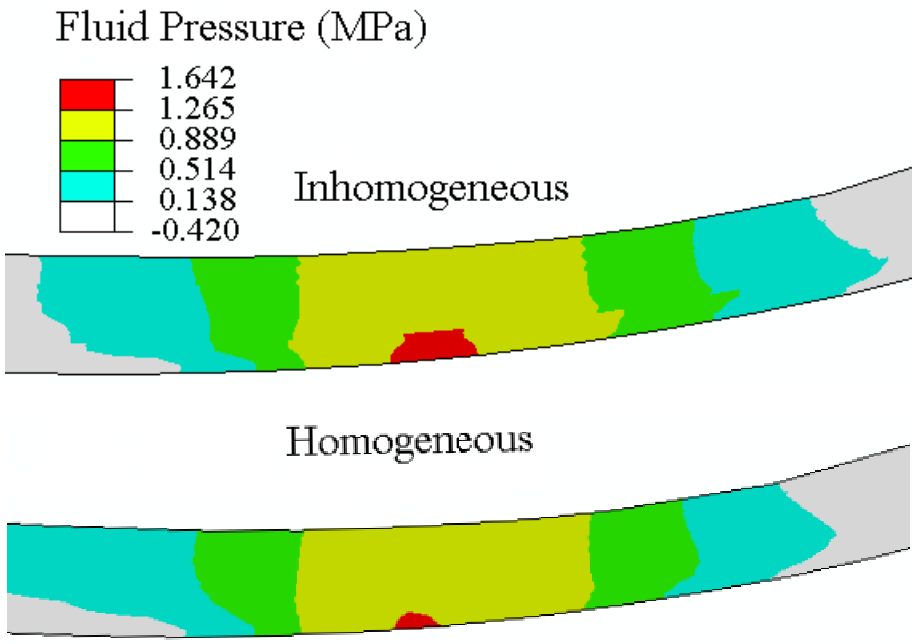
Fluid Pressure (MPa)
1.642
1.265
0.889
0.514
0.138
-0.420
Inhomogeneous
Homogeneous

(a)

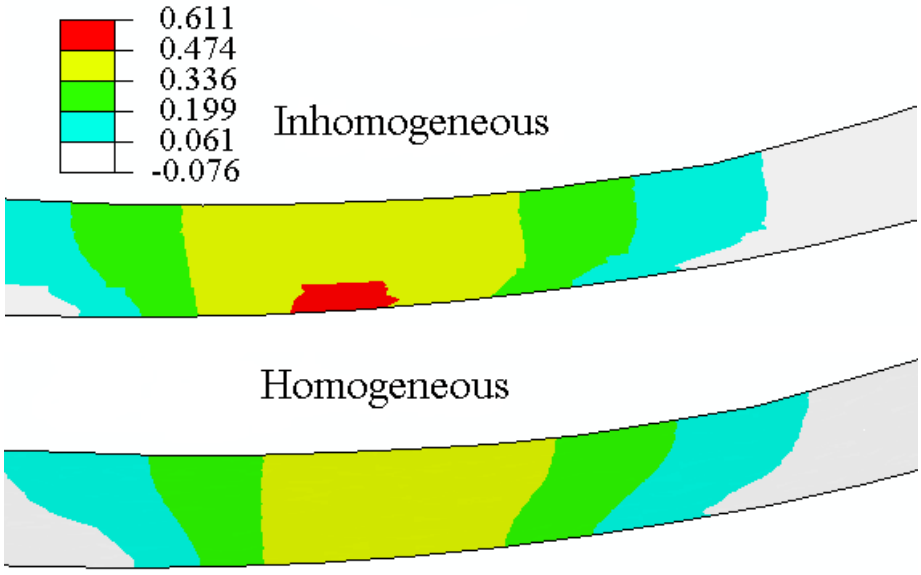
0.611
0.474
0.336
0.199
0.061
-0.076
Inhomogeneous
Homogeneous

(b)

Fig. 4

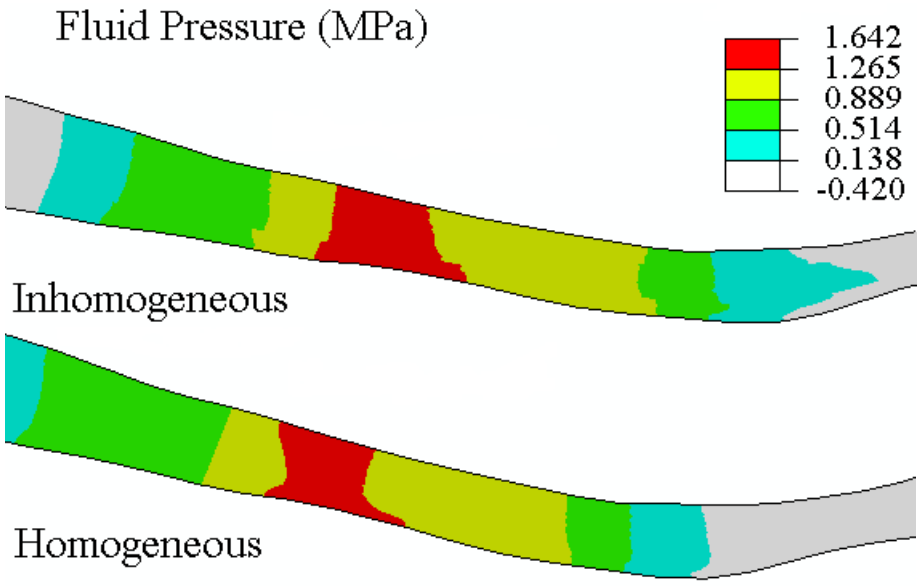
Fluid Pressure (MPa)
1.642
1.265
0.889
0.514
0.138
-0.420
Inhomogeneous
Homogeneous

(a)

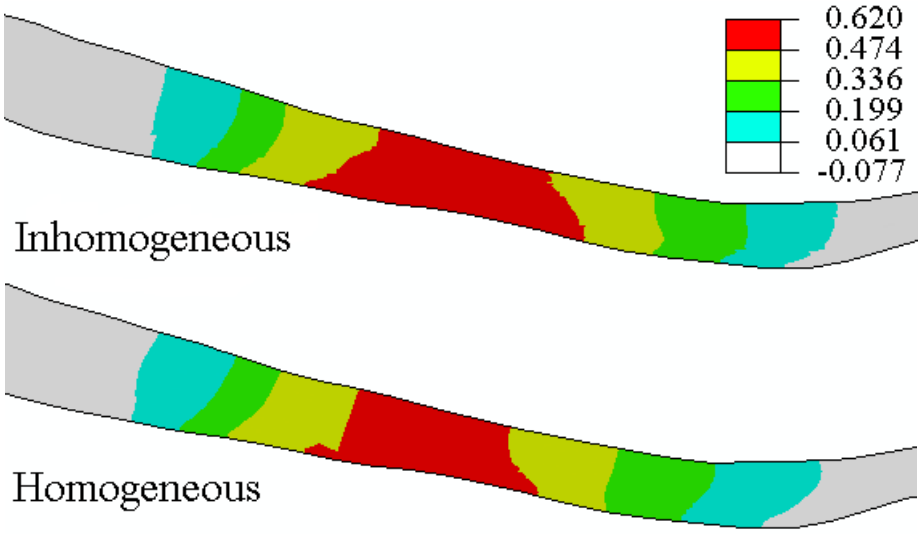
0.620
0.474
0.336
0.199
0.061
-0.077
Inhomogeneous
Homogeneous

(b)

Fig. 5

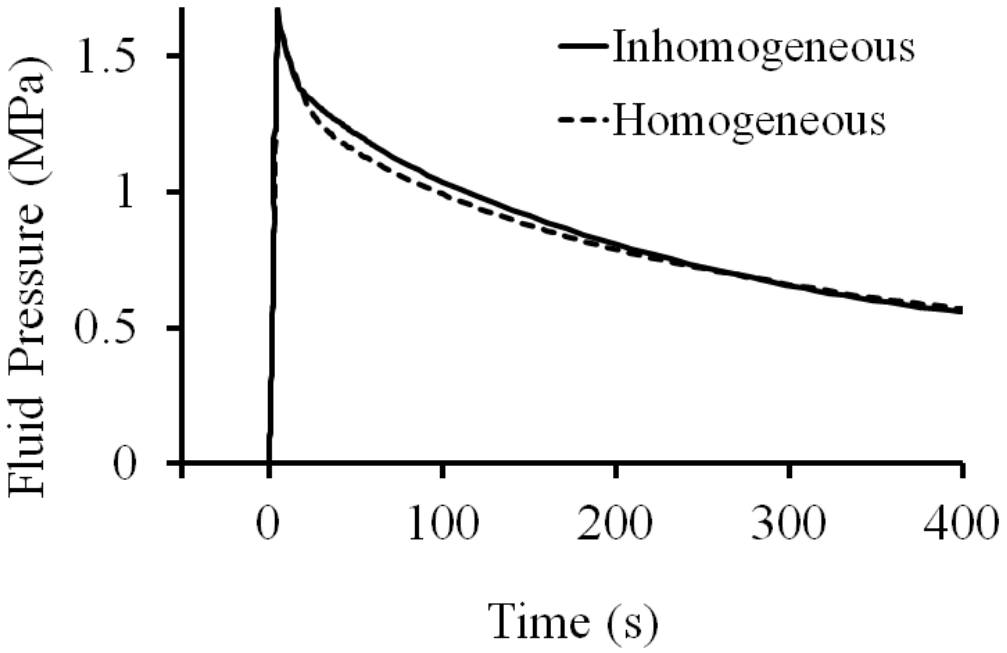
Inhomogeneous
Homogeneous
Fluid Pressure (MPa)
1.5
1
0.5
0
0
100
200
300
400
Time (s)

(a)

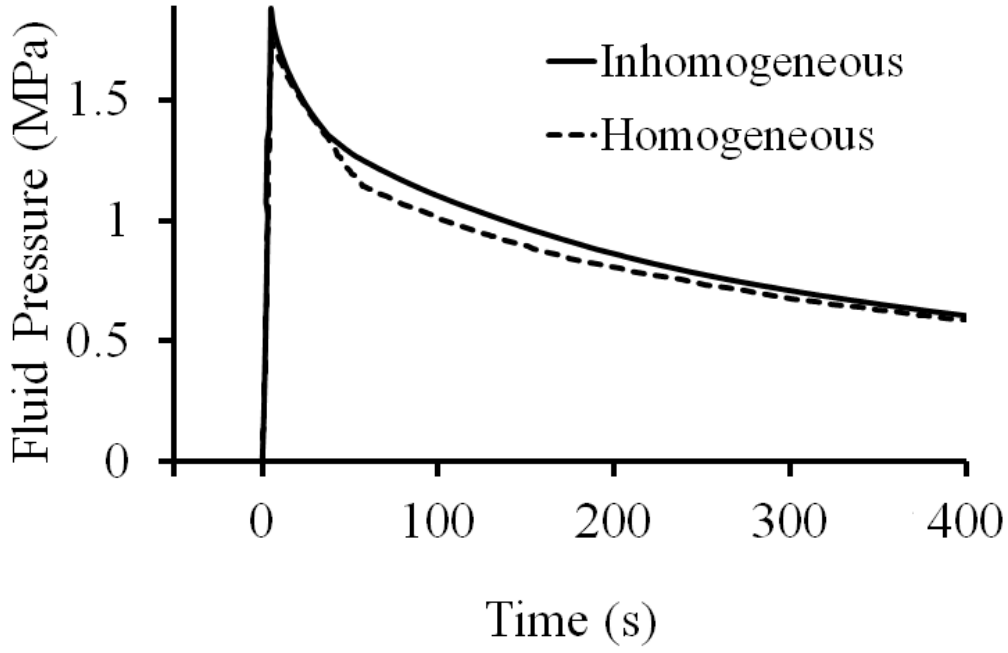
Inhomogeneous
Homogeneous
Fluid Pressure (MPa)
1.5
1
0.5
0
0
100
200
300
400
Time (s)

(b)

Fig. 6

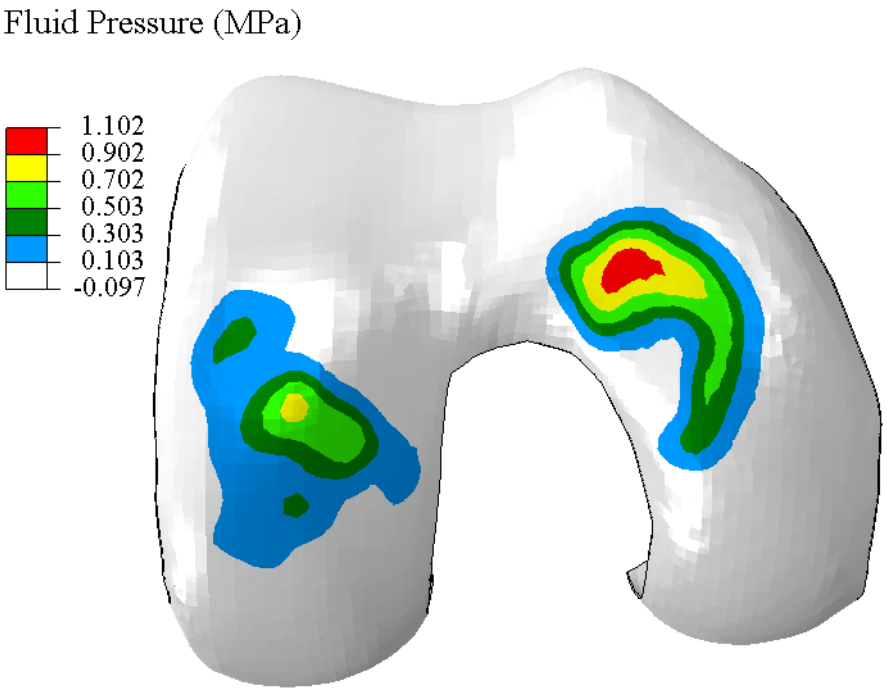

(a)

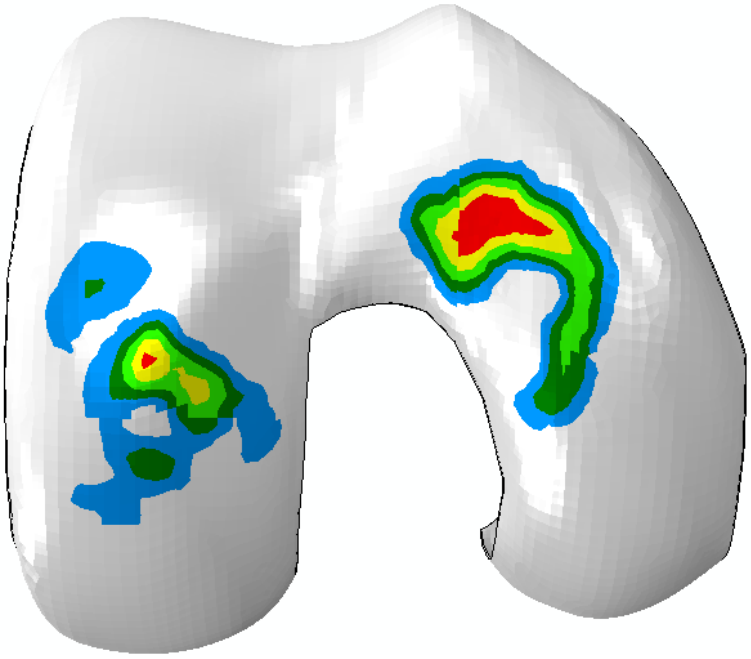

(b)

Fig. 7

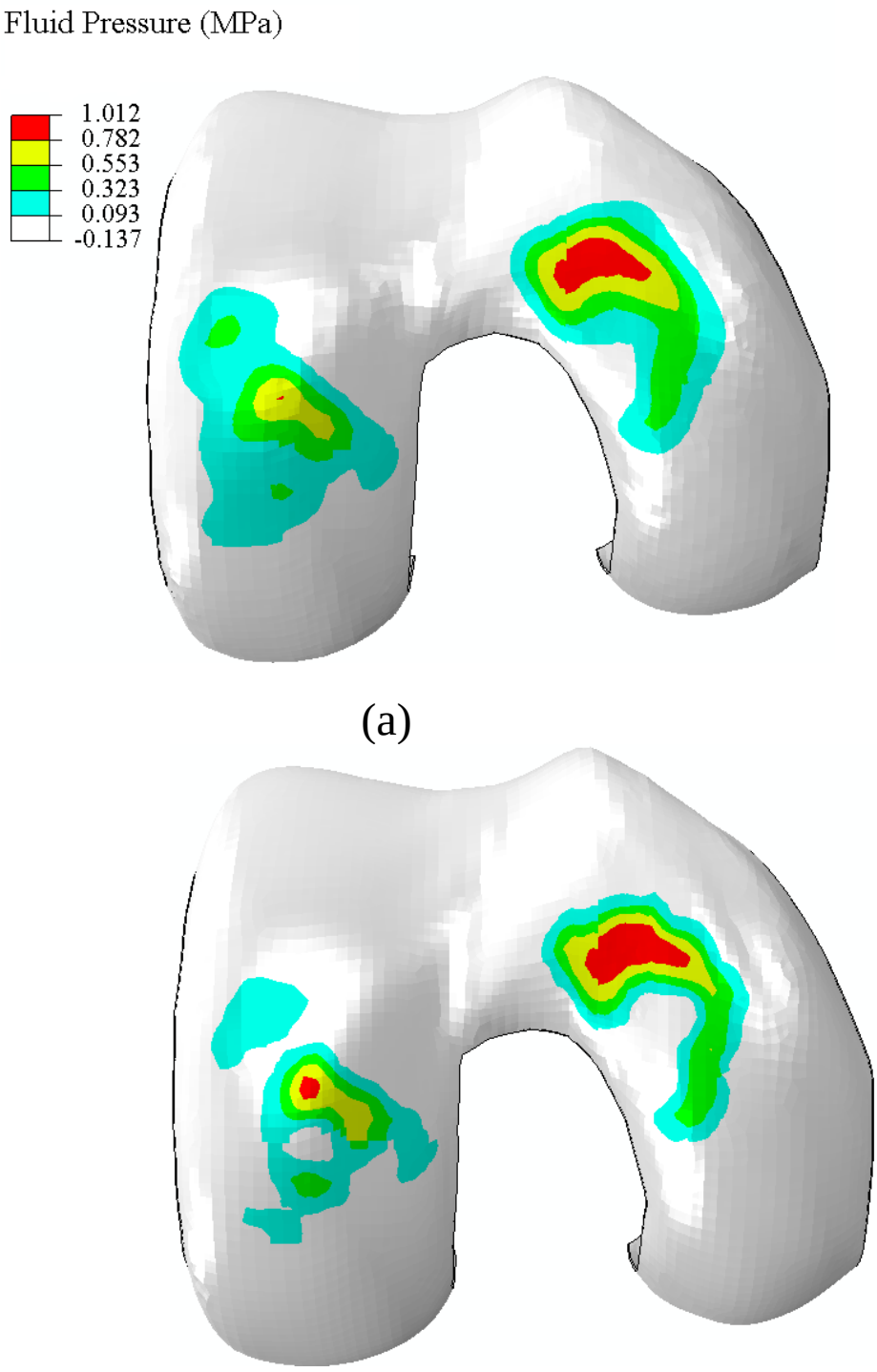

Fig. 8